IOP Publishing Journal of Physics: Condensed Matter
J. Phys.: Condens. Matter **29** (2017) 395504 (7pp) https://doi.org/10.1088/1361-648X/aa80b1

Stability, electronic and phononic properties of β and 1T structures of $SiTe_x$ ($x = 1, 2$) and their vertical heterostructures

A Kandemir[1], F Iyikanat[2] and H Sahin[3,4]

[1] Department of Materials Science and Engineering, Izmir Institute of Technology, 35430, Izmir, Turkey
[2] Department of Physics, Izmir Institute of Technology, 35430, Izmir, Turkey
[3] Department of Photonics, Izmir Institute of Technology, 35430, Izmir, Turkey
[4] ICTP-ECAR Eurasian Center for Advanced Research, Izmir Institute of Technology, 35430, Izmir, Turkey

E-mail: alikandemir@iyte.edu.tr and hasansahin@iyte.edu.tr

Received 17 May 2017, revised 10 July 2017
Accepted for publication 19 July 2017
Published 29 August 2017

Abstract

By performing first-principles calculations, we predict a novel, stable single layer phase of silicon ditelluride, 1T-$SiTe_2$, and its possible vertical heterostructures with single layer β-SiTe. Structural optimization and phonon calculations reveal that 1T-$SiTe_2$ structure has a dynamically stable ground state. Further analysis of the vibrational spectrum at the Γ point shows that single layer 1T-$SiTe_2$ has characteristic phonon modes at 80, 149, 191 and 294 cm^{-1}. Electronic-band structure demonstrates that 1T-$SiTe_2$ phase exhibits a nonmagnetic metallic ground state with a negligible intrinsic spin–orbit splitting. Moreover, it is shown that similar structural parameters of 1T-$SiTe_2$ and existing β-SiTe phases allows construction of 1T-β heterostructures with a negligible lattice mismatch. In this regard, it is found that two energetically favorable stacking orders, namely AA and A^TB, have distinctive shear and layer breathing phonon modes. It is important to note that the combination of semiconducting β-SiTe and metallic 1T-$SiTe_2$ building blocks forms ultra-thin Schottky barriers that can be used in nanoscale optoelectronic device technologies.

Keywords: vertical heterostructures, Schottky barrier, $SiTe_2$ monolayer, silicon-based nanomaterials

(Some figures may appear in colour only in the online journal)

1. Introduction

Following the synthesis of graphene [1, 2], two-dimensional (2D) materials have drawn extraordinary attention in different subfields of materials science and nanotechnology. In the last decade, novel 2D materials such as hexagonal boron nitride (h-BN) [3–5], silicene [6, 7], germanene [6, 8], transition metal dichalcogenides (TMDs) [9–15] phosphorene [16–18], stanene [19, 20] group III [21–23] and group IV monochalgenides [24–26] have been successfully synthesized.

Recent research efforts have shown that unique properties of 2D crystal structures can be enhanced by construction of their lateral and vertical heterostructures [27]. For instance, vertical heterostructures comprised of graphene and TMDs have been reported to be efficient phototransistors [28]. It has also been shown that vertically stacked graphene/h-BN heterostructures can be tailored as controllable electronic devices due to large band gap of h-BN [29, 30]. Synthesis of many other vertical heterostructures such as GaSe/graphene [31], WS_2/MoS_2 [32], $MoSe_2/Bi_2Se_3$ [33], $VSe_2/GeSe_2$ [34] and $MoSe_2/HfSe_2$ [35] have been reported, recently. In addition to bilayer heterostructures of 2D materials, three-layer heterostructures of them have also been achieved. Lin *et al* have reported successfully syntheses of $WSe_2/MoSe_2$/graphene and MoS_2/WSe_2/graphene heterostructures and shown that resonant tunneling Characteristics of the heterostructures can

be tuned by modifying the stacking order [36]. Furthermore, lateral heterostructures have been the focus of interest as another type of constructing different 2D materials. Recently, Li *et al* have reported epitaxial growth of MoS_2/WSe_2 lateral heterostructure and showed that lateral heterostructure has p-n junction properties can be used as 2D transistor [37]. Also different combinations of lateral heterostructures TMDs such as MoS_2/WS_2 [32], $MoSe_2/WSe_2$ [38] have been extensively studied. In addition to experimental studies, theoretical studies have predicted possible heterostructures of new synthesized single 2D materials, such as $Mg(OH)_2$–WS_2 and h-AlN/$Mg(OH)_2$ [39, 40].

Bulk silicon telluride is a p-type semiconductor with an indirect gap near 1 eV and direct gap near 2 eV. Keuleyan *et al* have reported synthesis of layered nano structures of Si_2Te_3 and showed variability of production methods [41]. Afterwards, Shen *et al* have investigated theoretically structural and electronic properties of bulk and various single layer form of Si_2Te_3 [42]. It can be avowable that monolayer of Si_2Te_3 has complex and thick structure. Another layered structure of silicon telluride has also been discovered by Saito *et al* [43]. While they investigated phase-change superlattices, layered Si_2Te_2 structure was found in experiments and also tried to explain the structure with theoretical simulations. Thereafter, Ma *et al* have shown free-standing single layer form of Si_2Te_2 is thermally and dynamically stable [44]. Additionally, by virtue of interesting electronic properties, Si_2Te_2 have been proposed as 2D topological insulator. Moreover, SiTe single layers as phosphorene analogues have been proposed by Chen *et al* [45]. They have predicted α- and β-SiTe single layers which are dynamically stable and 2D semiconductors.

In this paper, we presented unexplored stable 2D silicon ditelluride phase, 1T-$SiTe_2$. Structural, electronic and vibrational properties of novel single layer 1T-$SiTe_2$ were investigated with a stable single layer β-SiTe. Specifically, we envisioned structurally perfect consistence between the 1T-$SiTe_2$ and β-SiTe single layers. This is followed by stacking formations of the 1T-$SiTe_2$ and β-SiTe single layers, and hence the properties of possible vertical heterostructures were also studied in detail. Rest of the paper is organized as follows: Computational Methodology is given in section 2. The structural, electronic and vibrational properties of single layer structures of 1T-$SiTe_2$ and β-SiTe are presented in section 3. Vertical heterostructures and possible stacking formations are presented in section 4 with structural, electronic and vibrational analyses. Section 5 is devoted to conclusion of our results.

2. Computational methodology

First-principle calculations are performed using the plane-wave basis projector-augmented wave (PAW) method as implemented in the vienna *ab initio* simulation package (VASP) [46, 47]. The exchange-correlation energy was described by the generalized gradient approximation (GGA) using the Perdew–Burke–Ernzerhof (PBE) functional [48]. The van der Waals (vdW) correction to the GGA functional was included by using the DFT-D2 method of Grimme [49].

A plane-wave basis set with kinetic energy cutoff of 500 eV was used for all the calculations. The total energy difference between the sequential steps in the iterations was taken to be 10^{-5} eV for the convergence criterion. The total force in the unitcell was reduced to a value of less than 10^{-4} eV Å^{-1}. To hinder interactions between the adjacent cells, at least 12 Å vacuum space was used along the z-direction. All calculations were performed with spin polarized case. Analysis of the charge transfers in the structures was determined by the Bader technique [50]. The vibrational properties were obtained via PHONOPY code [51] that use the force constants calculated by finite-displacement method.

3. Structural, electronic and vibrational properties of single layer 1T-$SiTe_2$ and β-SiTe

Although it is one of the most common crystal structure for ultra-thin 2D materials, stability and characteristic properties of 1T phase have never been questioned before for silicon ditelluride. 1T-phase can be synthesized via further Tellurium doping of well-known β-SiTe phase. In this section, structural, electronic and vibrational properties of single layer 1T-$SiTe_2$ (and β-SiTe for comparison) are investigated in detail.

The β-SiTe is a buckled single layer structure composed of two layers, Si layer and Te layer, and has a hexagonal unit cell. The β-SiTe 2D crystal structure was shown in figure 1(a). The calculated lattice parameters for single layer β-SiTe are $a = b = 3.82$ Å . The thickness of single layer β-SiTe, which is defined to be the vertical distance between uppermost and lowermost atoms, was calculated to be 1.53 Å . The bond length between Si and Te atoms in the β-SiTe was calculated to be 2.69 Å . Moreover, Bader charge analysis shows that each Si atom donates 0.8 e and, as previously showed, each Te atom receives 0.4 e in the single layer β-SiTe, which is formed mostly with ionic bonds.

Figure 1(b) shows 1T structure for the predicted single layer silicon ditelluride, 1T-$SiTe_2$. The structure of single layer 1T-$SiTe_2$ has a hexagonal unit cell with lattice vectors, $a = b$, and the 1T-$SiTe_2$ is composed of three atom layers with Si layer sandwiched between two Te layers. As shown in the figure 1, the 1T-$SiTe_2$ phase resembles Te-doped single layer β-SiTe. Lattice constants of primitive unit cell of the 1T-$SiTe_2$ structure were calculated to be $a = b = 3.79$ Å . Moreover, the thickness of single layer of the 1T-$SiTe_2$ was calculated to be 3.25 Å . The bond length of Si–Te bonds in the 1T-$SiTe_2$ single layer was found to be 2.73 Å . Furthermore, Bader charge analysis for the 1T-$SiTe_2$ single layer shows that each Si atom donates 0.6 e and each Te atom receives 0.3 e. It seems that ionic character is more dominant than covalent character in the bonds of 1T-$SiTe_2$.

To benchmark the structural findings, table 1 shows structural properties of the single layer $SiTe_x$ phases. Besides the geometric similarity of the $SiTe_x$ phases, it was also found that the ground states of 1T-$SiTe_2$ and β-SiTe single layers are non-magnetic. In addition, cohesive energies of the 1T-$SiTe_2$ and β-SiTe single layers were calculated to be 3.34 and 3.38 eV/atom, respectively. It indicates that both single layers are located similar equilibrium states with a strong crystallization

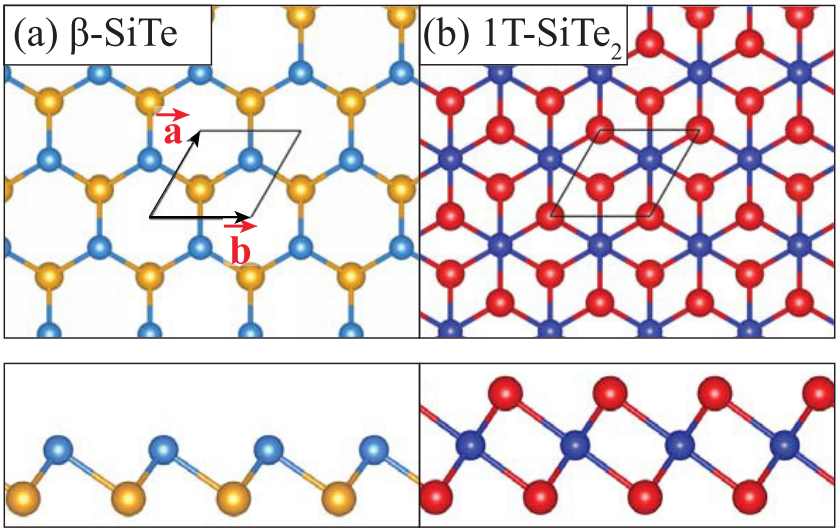

Figure 1. Top and side views of geometric structures of (a) β-SiTe and (b) 1T-$SiTe_2$. Turquoise/blue and orange/red atoms show Si and Te atoms, respectively.

Table 1. The calculated ground state properties of single layer structures of 1T-$SiTe_2$ and β-SiTe: phase, lattice parameter of primitive unit cell, a and b; the distance between Si and Te atoms,d_{Si-Te}; thickness of single layer, t, magnetic state; the total amount of charge received by the Te atoms, $\Delta\rho$; the cohesive energy per atom in the unitcell, E_c; the energy band gap of the structure calculated within GGA(E_g), GGA + SOC(E_g^{SOC}) and workfunction, Φ, for 1T-$SiTe_2$ it is same for both surface side, for β-SiTe it is determined Si side and Te side, $\Phi1$ and $\Phi2$, respectively; The in-plane stiffness, C, and Poisson's ratio, ν . NM denotes non-magnetic.

Phase	a (Å)	b (Å)	d_{Si-Te} (Å)	t (Å)	Magnetic State	$\Delta\rho$ (e)	E_c (eV/atom)	E_g (eV)	E_g^{SOC} (eV)	Φ_1 (eV)	Φ_2 (eV)	C (N m^{-1})	ν
1T-$SiTe_2$	3.79	3.79	2.73	3.25	NM	0.3	3.34	—	—	4.84	4.84	46.4	0.55
β-SiTe	3.82	3.82	2.69	1.53	NM	0.4	3.38	1.79	1.51	5.43	5.28	39.6	0.20

energy. We emphasize that the 1T-$SiTe_2$ and β-SiTe single layers are structurally well compatible to each other.

The in-plane stiffness, C, and Poisson's ratio, ν, of the single layer $SiTe_x$ phases were also investigated. Methodology of Yagmurcukardes *et al* [52] was used to obtain elastic constans of the single layer $SiTe_x$ phases. It was calculated that in-plane stiffness of 1T-$SiTe_2$ and β-SiTe are 46.4 and 39.6 N m^{-1}, respectively. It appears that the in-plane stiffness values of $SiTe_x$ single layers are much lower than well-known 2D materials, such as graphene (300–340 N m^{-1}) [52–54], MoS_2 (120–180 N m^{-1}) [52, 55, 56] and $MoSe_2$ (98–103 N m^{-1}) [56, 57]. The calculated Poisson's ratio values for 1T-$SiTe_2$ and β-SiTe are 0.55 and 0.20, respectively. Considering a number of 1T and 2H phase 2D materials, Poisson's ratio values are in the range between 0.18 and 0.25 [56, 58]. Contrary to expectations, Poisson's ratio of 1T-$SiTe_2$ phase is almost three times higher than other 1T phase 2D structures.

Our results for the phonon dispersion curves of the 1T-$SiTe_2$ and β-SiTe 2D crystal structures are shown in figure 2. There are one Si atom and one Te atom within the primitive unit cell of dynamically stable β-SiTe phase and its phonon spectrum includes 6 phonon branches, 3 acoustic and 3 optical. Optical phonons include one doubly degenerate in-plane vibrational mode at 245 cm^{-1} and one singly degenerate out-of-plane vibrational mode at 335 cm^{-1}. Our calculations on vibrational properties of the 1T-$SiTe_2$ phase reveal the dynamical stability of the 1T structure. In the primitive unit cell of 1T-$SiTe_2$, there are one Si atom and two Te atoms and its phonon spectrum includes 9 phonon branches, 3 acoustic and 6 optical. Optical phonons include two doubly degenerate in-plane vibrational modes at 80 cm^{-1}, 191 cm^{-1} and two singly degenerate out-of-plane vibrational modes at 149 cm^{-1} and 294 cm^{-1}. Characteristics of four optical modes of the 1T-$SiTe_2$ and two optical modes of the β-SiTe at Γ are shown in figure 2. In addition, a large and moderate phonon energy band gaps are found between phonon modes in β-SiTe and 1T-$SiTe_2$ single layers, respectively. The large phonon band gap in β-SiTe obstruct contact of the acoustic modes and the optical modes, whereas the moderate phonon band gap separates the optical modes with or without contribution of Si atoms. On the other hand, the single layers of 1T-$SiTe_2$ and β-SiTe possess low frequency vibrational modes. It appears that both of the phases are soft 2D materials compared to other 2D materials such as graphene, silicene, h-BN, etc.

The calculated electronic band structures of single layer silicon tellurides are shown in figure 3. It is found that β-SiTe single layer is a semiconductor with indirect band gap with its valence band maximum (VBM) residing at Γ point and conduction band minimum (CBM) within Γ-M point. Consistent with previous result [45], the band gap of single layer β-SiTe was calculated to be 1.79 eV. Calculations included spin–orbit interactions showed that the band gap of single layer

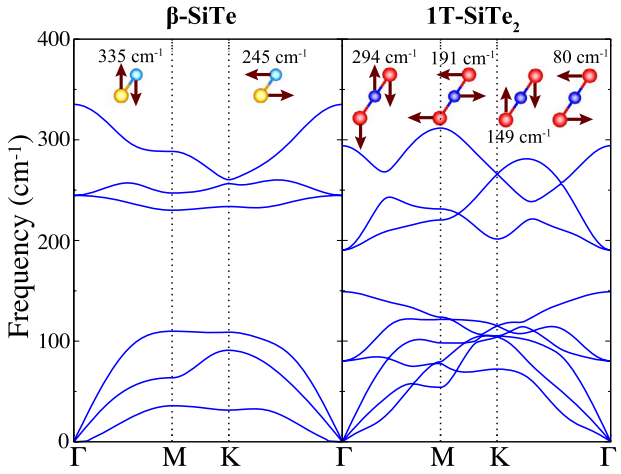

Figure 2. Phonon band structures of β-SiTe and 1T-$SiTe_2$ single layers. Side views of eigenvectors correspond to related optical phonon modes are also shown.

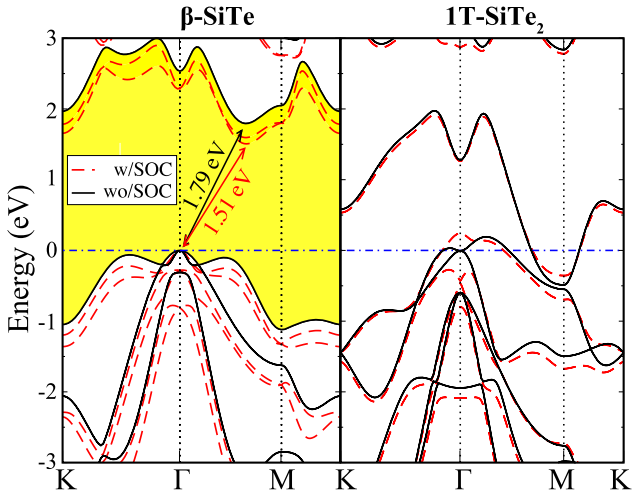

Figure 3. Electronic band diagrams of β-SiTe and 1T-$SiTe_2$ single layers with and without spin–orbit interactions. Fermi level is set to zero.

β-SiTe decreases to 1.51 eV and the band edges of CBM and VBM does not change. With the effect of spin–orbit coupling (SOC), double degenerate VBM is separated at Γ point about 283 meV in the β-SiTe and also CBM splits 89 meV at the point between Γ and M.

As shown in the figure 3, metallic electronic band structure of the single layer 1T-$SiTe_2$ was obtained. Moreover, two different energy bands cross Fermi level at four different points in k-space of the 1T-$SiTe_2$. Degeneracy of the maximum occupied electronic states is separated at Γ point about 672 meV due to SOC effect in the 1T-$SiTe_2$. Conspicuously, no splitting occurs for bands in all Brillouin Zone of the 1T-$SiTe_2$ by virtue of the presence of inversion symmetry in 1T phase. It was observed that dispersion characteristic in the 1T-$SiTe_2$ only differs around Γ point with the effect of SOC.

4. Vertical Heterostructures of 1T-$SiTe_2$ and β-SiTe

Structural similarity and electronic diversity of the 1T-$SiTe_2$ and β-SiTe phases promise unusual properties with clean interface for vertical heterostructures. Therefore, investigation of structural, electronic and vibrational properties of different stacked vertical heterostructures is essential.

To determine energetically favorable bilayer heterostructure, four different stacking orders are considered. Possible stacking formations; AA (Si atoms of β-SiTe and 1T-$SiTe_2$ coincide laterally), AB (Si atoms of β-SiTe coincide laterally to Te atoms of the 1T-$SiTe_2$ at the interface), A^TA (transposed β-SiTe like AA) and A^TB (transposed β-SiTe like AB) are shown in figure 4, respectively. In table 2, structural properties of bilayer silicon telluride heterostructures are given. Lattice constants of all bilayer stackings were expected to be between the lattice constants of β-SiTe and 1T-$SiTe_2$. However, AA stacking has lattice constant of 3.85 Å , whereas others stackings have lattice constant of 3.80 Å . Layer-layer distance of AA stacking is the lowest one, 2.26 Å , compared to other stackings. It appears that strong inter-planar interaction in AA stacking order weakens intra-planar bonds and increases in lattice constant. The distance of nearest atoms between the bilayer is 3.17 Å , which is 16% higher than the Si-Te bond distance of the $SiTe_x$ phases. We argue that Si and Te atoms at the interface layers binds together with strong non-covalent interaction instead of a Si-Te bond. Moreover, layer-layer distances of AB, A^TA and A^TB stackings were calculated to be 3.92, 4.02 and 3.43 Å and the closest bond distance between layers in these stackings showed that no primary bond occurs between bilayer.

Our electronic structure calculations show that AA stacking is the ground state stacking structure with the highest interlayer binding energy, 459 meV. In contrast, the lowest interlayer interaction energy between the layers in AB stacking is 116 meV. It is shown that, once Si layer of the β-SiTe is opposite neighbor layer for the 1T-$SiTe_2$, most favorable bilayer formation is AA stacking order. While Te layer of the β-SiTe is opposite neighbor layer for the 1T-$SiTe_2$, two different stackings, A^TA and A^TB, are found to be possible formations of vertical heterostructures. A^TB stacking has second favorable stacking among all stackings. Furthermore, A^TA stacking has 143 meV interlayer binding energy between layers. Compared to stacking orders, A^TB type stacking order is more favorable in transposed bilayer heterostructures. Bader charge analysis of vertical heterostructures showed that no remarkable differences in charge transfers of bilayer silicon tellurides stackings were observed compared to bare 1T-$SiTe_2$ and β-SiTe single layers. It can be said that dominant ionic intra-layer bond character does not change in the layers with the effect of vertical heterostructure formation.

Here, vibrational properties of the preferable vertical heterostructures are discussed. Phonon band diagrams of AA and A^TB stackings are represented in figure 5. The figure shows that favorable bilayer structures are dynamically stable. Due to insufficient FFT-grid, phonon band diagram of AA stacking has negative frequencies about Γ point for out-of-plane acoustic phonon mode. However, it is well-known that the out-of-plane acoustic phonon modes have quadratic dispersion in 2D materials. Therefore, we show quadratic-fitted curve for

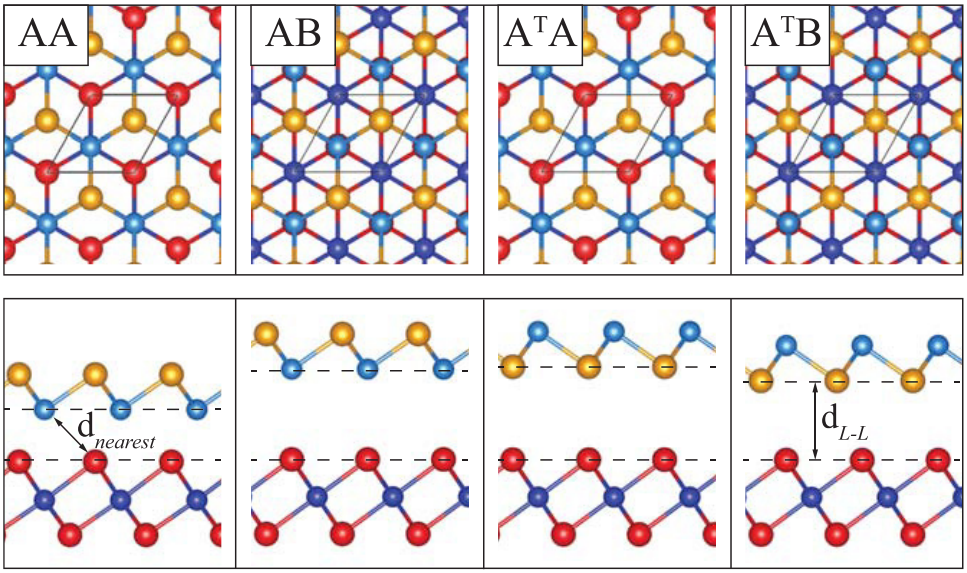

Figure 4. Top and side view of geometric structures of possible stacking formations of the vertical 2D silicon telluride structures.

Table 2. The stacking labels of vertical heterostructures of 2D silicon tellurides are given in the first column. Calculated parameters for bilayer heterostructures for 1T-$SiTe_2$ and β-SiTe are; lattice constant in the lateral direction, a and b; the interlayer distance, d_{L-L}; the energy difference between the ground state (AA stacking), ΔE; the interlayer interaction energy between the layers, E_{int}; the distance of nearest atoms between bilayer, d_{nearest}; the total amount of charge received by the Te atoms in β-SiTe and 1T-$SiTe_2$, $\Delta\rho_\beta$ and $\Delta\rho_{1T}$, respectively.

	a (Å)	b (Å)	d_{L-L} (Å)	d_{nearest} (Å)	ΔE(meV)	E_{int} (meV)	$\Delta\rho_\beta$ (e)	$\Delta\rho_{1T}$ (e)
AA	3.85	3.85	2.26	3.17	0	459	0.4	0.3
AB	3.80	3.80	3.92	3.92	344	116	0.4	0.3
A^TA	3.80	3.80	4.02	4.02	317	143	0.4	0.3
A^TB	3.80	3.80	3.43	4.07	233	236	0.4	0.3

out-of-plane acoustic phonon mode in the phonon band structure of AA stacking. The presence of optical phonon branches that have quite low eigenvalues is another direct indication of the soft materials of the bilayer silicon telluride 2D structures. The vertical stackings maintain phonon band gaps of the single layer silicon tellurides. Especially, phonon band diagram of A^TB stacking is superposition of the β-SiTe and 1T-$SiTe_2$ phonon band diagrams.

We further analyse the phonon spectrums of favorable vertical heterostructures. When the β-SiTe/1T-$SiTe_2$ vertical heterostructure is formed, two characteristic phonon modes, layer breathing mode (LBM) and shear mode (SM) appear in the phonon spectrum. Eigenvectors of LBM and SM for AA and A^TB bilayer structures are shown in the figure 5. LBM modes for AA and A^TB bilayer structures are found with frequencies of 72 and 41 cm^{-1}, respectively. As a consequence of strong interlayer interaction between the β-SiTe and 1T-$SiTe_2$ phases, frequency of the LBM in AA stacking is much higher than that of A^TB stacking. In addition, eigenfrequency of SM in AA and A^TB heterostructures are found to be 3.4 and 20 cm^{-1}, respectively. However, it is seen that in contrast to strong interlayer interaction, sliding of layers in AA stacking is much easier. Phonon calculations reveal that both AA and A^TB vertical heterostructures are stable

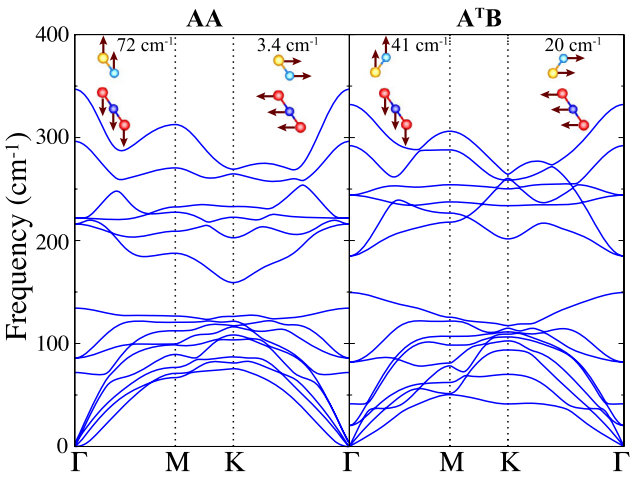

Figure 5. Phonon band structures of AA and A^TB stackings. Side views of eigenvectors corresponds to shear and layer breathing modes are also shown.

and clearly distinguishable due to their characteristic LBM and SM.

Electronically, all vertical heterostructures are found to exhibit metallic behavior because of the contribution of

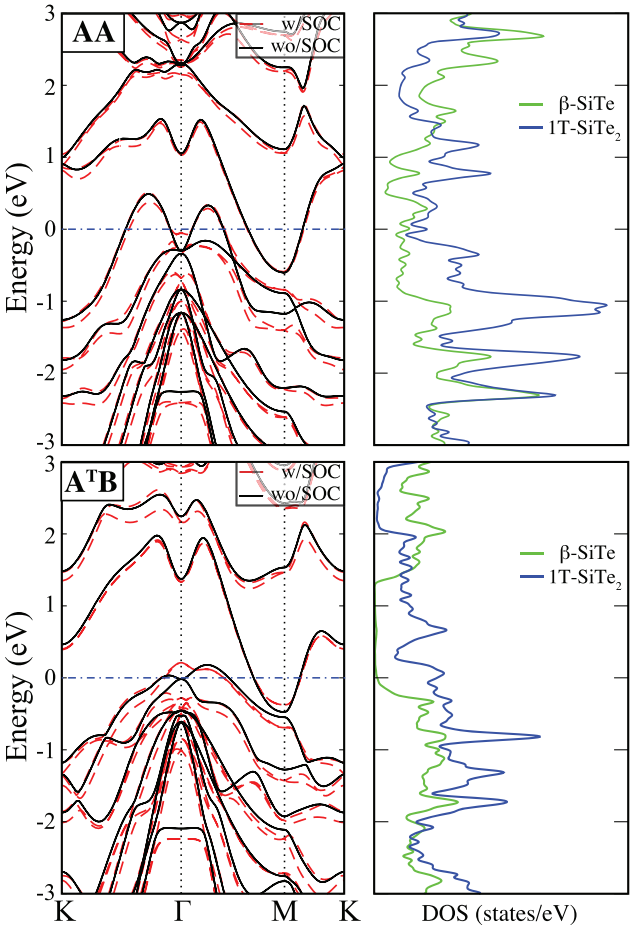

Figure 6. Electronic band diagrams and density of states of AA and A^TB stackings. Fermi level is set to zero.

single layer 1T-$SiTe_2$ (figure 6). It can be seen that electronic band diagram shows AA bilayer heterostructure is metal and maximum occupied electronic state moves to within K and Γ point, which is not observed in previous electronic band diagrams. It seems that strong interaction between layers in AA stacking strongly modifies the electronic band diagram. Moreover, stacking partially visualized density of states show that metallization of β-SiTe single layer is formed by contribution from 1T phase. As shown in the figure 6, electronic band diagram of the A^TB stacking, which is superposed the electronic band diagrams of 1T-$SiTe_2$ and β-SiTe, shows that interaction between layers in the A^TB stacking is van der Waals type interaction. However, it is also seen that β-SiTe has contribution to near Fermi level (left side of Γ) and the density of states shows that β-SiTe is also metallized in A^TB stacking order.

To gain further insights into the vertical heterostructures, we model electronic contact mechanisms of the favorable stackings. Since β-SiTe is a semiconductor with indirect band gap and 1T-$SiTe_2$ is metal, it looks like possible to produce 2D vertical heterostructures that form a Schottky barrier. Moreover, workfunctions of β-SiTe and 1T-$SiTe_2$ were determined. Figure 7 shows that workfunction values of β-SiTe (Si-Side), β-SiTe (Te-Side) and 1T-$SiTe_2$ which are 5.43, 5.28 and 4.84 eV, respectively. In the view of such information, to clarify contact region behavior while vertical heterostructure

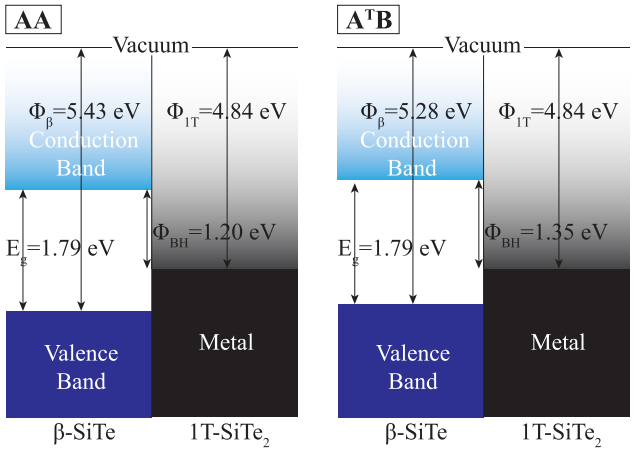

Figure 7. Schematic energy diagram of possible vertical heterostructures, AA and A^TB stackings, respectively. Barrier height of junction, Φ_{BH}; workfunction of β-SiTe, Φ_β; workfunction of 1T-$SiTe_2$, Φ_{1T}.

is formed, figure 7 shows schematic energy diagrams of the two favorable stacked vertical heterostructures. As shown in figure 7, vertical heterostructures of the single layer silicon tellurides forms a Schottky contact. Hereby, metal 1T-$SiTe_2$ phase tends to lose electrons to the semiconductor β-SiTe phase, because the Fermi level is lower in the semiconductor. With the generation of low energy bands at contact region, intrinsic semiconductor β-SiTe becomes p-type semiconductor. Findings revealed that by using only Si and Te atoms, it is possible to produce both semiconductor and metal single layers, moreover, this opportunity allows to fabricate nanostructural designs.

5. Conclusions

In conclusion, we studied structural, phononic and electronic properties of a novel stable structure of silicon telluride. It was found that 1T phase of silicon ditelluride has a dynamically stable crystal structure that resembles Te-doped β-SiTe phase. Analysis of the phonon spectrum of single layer 1T-$SiTe_2$ showed that it has characteristic vibrational zone center phonon modes at 80, 149, 191 and 294 cm^{-1}. Electronically, single layer 1T-$SiTe_2$ structure displays metallic behavior.

In addition, it was shown that structural similarity between 1T-$SiTe_2$ and β-SiTe also opens up the possibility of formation of vertical heterostructures. Two possible stacking orders between 1T-$SiTe_2$ and β-SiTe, AA and A^TB, were found to be energetically favorable and dynamically stable. Further analyses of the phonon spectrum revealed that these two stackings have characteristic shear and layer breathing modes that provide possible fingerprints of the heterostructures for the identification in Raman spectroscopy measurements. It was also predicted that the vertical heterostructure of 1T-$SiTe_2$ and β-SiTe may serve as an ultra-thin Schottky barrier with a perfect interface. It appears that single layer 1T-$SiTe_2$ crystal with its metallic nature is a suitable nanoscale electrode and a promising building block for ultra-thin Schottky diode applications.

Acknowledgments

Computational resources were provided by TUBITAK ULAKBIM, High Performance and Grid Computing Center (TR-Grid e-Infrastructure). HS acknowledges financial support from the TUBITAK under the project number 116C073. FI acknowledges financial support from the TUBITAK under the project number 114F397. HS acknowledges support from Bilim Akademisi-The Science Academy, Turkey under the BAGEP program.

ORCID iDs

A Kandemir https://orcid.org/0000-0001-9813-6421

References

[1] Novoselov K S, Geim A K, Morozov S V, Jiang D, Zhang Y, Dubonos S V, Grigorieva I V and Firsov A A 2004 *Science* **306** 666
[2] Geim A K and Novoselov K S 2007 *Nat. Mater.* **6** 183
[3] Pacile D, Meyer J C, Girit Ç Ö and Zettl A 2008 *Appl. Phys. Lett.* **92** 133107
[4] Han W Q, Wu L, Zhu Y, Watanabe K and Taniguchi T 2008 *Appl. Phys. Lett.* **93** 223103
[5] Kim K K *et al* 2012 *Nano Lett.* **12** 161
[6] Cahangirov S, Topsakal M, Aktürk E, Sahin H and Ciraci S 2009 *Phys. Rev. Lett.* **102** 236804
[7] Vogt P *et al* 2012 *Phys. Rev. Lett.* **108** 155501
[8] Davila M E, Xian L, Cahangirov S, Rubio A and Lay G L 2014 *New J. Phys.* **16** 095002
[9] Gordon R A, Yang D, Crozier E D, Jiang D T and Frindt R F 2002 *Phys. Rev.* B **65** 125407
[10] Mak K F, Lee C, Hone J, Shan J and Heinz T F 2010 *Phys. Rev. Lett.* **105** 136805
[11] Coleman J N *et al* 2011 *Science* **331** 568
[12] Wang Q H, Kalantar-Zadeh K, Kis A, Coleman J N and Strano M S 2012 *Nat. Nanotechnol.* **7** 699
[13] Sahin H, Tongay S, Horzum S, Fan W, Zhou J, Li J, Wu J and Peeters F M 2013 *Phys. Rev.* B **87** 165409
[14] Ross J S *et al* 2014 *Nat. Nanotechnol.* **9** 268
[15] Chen B, Sahin H, Suslu A, Ding L, Bertoni M I, Peeters F M and Tongay S 2015 *ACS Nano* **9** 5326
[16] Liu H, Neal A T, Zhu Z, Luo Z, Xu X, Tomanek D and Ye P D 2014 *ACS Nano* **8** 4033
[17] Zhu Z and Tomanek D 2014 *Phys. Rev. Lett.* **112** 176802
[18] Carvalho A, Wang M, Zhu X, Rodin A S, Su H and Neto A H C 2016 *Nat. Rev. Mater.* **1** 16061
[19] Zhu F F *et al* 2015 *Nat. Mater.* **14** 1020
[20] Saxena S, Chaudhary R P and Shukla S 2016 *Sci. Rep.* **6** 31073
[21] Hu P, Wen Z, Wang L, Tan P and Xiao K 2012 *ACS Nano* **6** 5988
[22] Hu P *et al* 2013 *Nano Lett.* **13** 1649
[23] Bandurin D A *et al* 2017 *Nat. Nanotechnol.* **12** 223
[24] Mukherjee B, Cai Y, Tan H R, Feng Y P, Tok E S and Sow C H 2013 *ACS Appl. Mater. Interfaces* **5** 9594
[25] Tritsaris G A, Malone B D and Kaxiras E 2013 *J. Appl. Phys.* **113** 233507
[26] Gomes L C and Carvalho A 2015 *Phys. Rev.* B **92** 085406
[27] Geim A K and Grigorieva I V 2013 *Nature* **499** 419
[28] Roy K, Padmanabhan M, Goswami S, Sai T P, Ramalingam G, Raghavan S and Ghosh A 2013 *Nat. Nanotechnol.* **8** 826
[29] Dean C R *et al* 2010 *Nat. Nanotechnol.* **5** 722
[30] Yang W *et al* 2013 *Nat. Mater.* **12** 792
[31] Li X *et al* 2015 *ACS Nano* **9** 8078
[32] Gong Y *et al* 2014 *Nat. Mater.* **13** 1135
[33] Xenogiannopoulou E *et al* 2015 *Nanoscale* **7** 7896
[34] Alemayehu M B, Falmbigl M, Ta K, Ditto J, Medlin D L and Johnson D C 2015 *Angew. Chem., Int. Ed.* **54** 15135
[35] Aretouli K E *et al* 2015 *Appl. Phys. Lett.* **106** 143105
[36] Lin Y C *et al* 2015 *Nat. Commun.* **6** 7311
[37] Li M Y *et al* 2015 *Science* **349** 524
[38] Huang C *et al* 2014 *Nat. Mater.* **13** 1096
[39] Yagmurcukardes M, Torun E, Senger R T, Peeters F M and Sahin H 2016 *Phys. Rev.* B **94** 195403
[40] Bacaksiz C, Dominguez A, Rubio A, Senger R T and Sahin H 2017 *Phys. Rev.* B **95** 075423
[41] Keuleyan S, Wang M, Chung F R, Commons J and Koski K J 2015 *Nano Lett.* **15** 2285
[42] Shen X, Puzyrev Y S, Combs C and Pantelides S T 2016 *Appl. Phys. Lett.* **109** 113104
[43] Saito Y, Tominaga J, Fons P, Kolobov A V and Nakano T 2014 *Phys. Status Solidi* **8** 302
[44] Ma Y, Kou L, Dai Y and Heine T 2016 *Phys. Rev.* B **94** 201104
[45] Chen Y, Sun Q and Jena P 2016 *J. Mater. Chem.* C **4** 6353
[46] Kresse G and Hafner J 1993 *Phys. Rev.* B **47** 558
[47] Kresse G and Furthmuller J 1996 *Phys. Rev.* B **54** 11169
[48] Perdew J P, Burke K and Ernzerhof M 1996 *Phys. Rev. Lett.* **77** 3865
[49] Grimme S 2006 *J. Comput. Chem.* **27** 1787
[50] Henkelman G, Arnaldsson A and Jonsson H 2006 *Comput. Mater. Sci.* **36** 354
[51] Togo A, Oba F and Tanaka I 2008 *Phys. Rev.* B **78** 134106
[52] Yagmurcukardes M, Senger R T, Peeters F M and Sahin H 2016 *Phys. Rev.* B **94** 245407
[53] Lee C, Wei X, Kysar J W and Hone J 2008 *Science* **321** 385
[54] Lee G-H *et al* 2013 *Science* **340** 1073
[55] Bertolazzi S, Brivio J and Kis A 2011 *ACS Nano* **5** 9703
[56] Kang J, Tongay S, Zhou J, Li J and Wu J 2013 *Appl. Phys. Lett.* **102** 012111
[57] Kandemir A, Yapicioglu H, Kinaci A, Çagın T and Sevik C 2016 *Nanotechnology* **27** 055703
[58] Guzman D M and Strachan A 2014 *J. Appl. Phys.* **115** 243701